Sputtering of Si nanospheres

Maureen L. Nietiadi,[1] Luis Sandoval,[2] Herbert M. Urbassek,[1,*] and Wolfhard Möller[3]

[1]*Physics Department and Research Center OPTIMAS, University Kaiserslautern, Erwin-Schrödinger-Straße, D-67663 Kaiserslautern, Germany*

[2]*Theoretical Division, Los Alamos National Laboratory, Los Alamos, New Mexico 87545, USA*

[3]*Institute of Ion Beam Physics and Materials Research, Helmholtz-Zentrum Dresden-Rossendorf, Bautzner Landstr. 400, D-01328 Dresden, Germany*

(Received 5 May 2014; revised manuscript received 2 July 2014; published 21 July 2014)

Spherical objects, such as clusters, nanoparticles, or aerosol particles, are sputtered when exposed to energetic irradiation. We use Monte Carlo (MC) and molecular dynamics (MD) computer simulation to study this process, with 20 keV Ar impact on a-Si clusters as a prototypical example. The sputter yield is quantified as being influenced by oblique incidence and target curvature. Cluster radii R are scaled to the energy deposition depth, a. For large R ($R/a > 5$) sphere sputtering follows closely the sputtering of planar targets, if the variation of the incidence angle on the sphere surface is taken into account. For smaller radii, the yield increases due to the influence of curvature. For radii $R/a \lesssim 1$ pronounced forward sputtering leads to a maximum in the sputter yield. For smaller R, sputter emission becomes isotropic, but decreases in magnitude since not all the projectile energy is deposited in the sphere. However, for all spheres studied ($R \geqslant 0.05a$) the average sputter yield is larger than for infinitely large spheres ($R \to \infty$). A simple model based on linear collision cascade theory and assuming that the energy deposition profile is independent of the sphere size predicts sputtering for large spheres well, but fails for small spheres where it strongly underestimates sputtering. The MC data for the smaller spheres are supplemented by MD calculations, which indicate a significant additional contribution caused by spike sputtering.

DOI: 10.1103/PhysRevB.90.045417 PACS number(s): 79.20.Rf, 79.20.Ap, 61.80.Lj

I. INTRODUCTION

If nanoparticles are exposed to an energetic particle flux, they may be sputtered. Such processes occur for example for dust particles in space [1,2] or in a plasma environment [3] and also for aerosols [4]. In other applications, ion irradiation is used to modify supported nanoparticles [5,6]. Sputtering of spherical objects is also of interest in more exotic environments, such as the sputtering of planetary atmospheres by magnetospheric plasmas or the solar wind [7].

Sputtering of spheres has been considered previously by molecular dynamics (MD) computer simulation for exemplary cases [8–11]. Järvi *et al.* [12,13] analyzed the sputtering of Au nanoparticles with radii up to 8 nm by 25 keV Ga ions using MD computer simulation; they also provide a theoretical evaluation, which results in a double integral that can only be evaluated numerically for specific cases. These authors also show that sputtering has a maximum as a function of sphere size. Monte Carlo (MC) simulations have been more rare; in their early work Jurac *et al.* showed that sputter yields increase when sphere size is reduced down to the projectile penetration depth [14].

Furthermore, the sputtering of nanostructures on surfaces such as nanodots or hillocks can be approximated by the sputtering of a spherical structure. Such nanostructures may be created by ion irradiation itself; it is known that prolonged ion irradiation may lead to the formation of nanopatterns such as ripples and dot structures [15,16].

Ion irradiation of nanowires and the effect of structure size on sputtering has been explored in several papers recently. Xue-Qing *et al.* [17] studied damage formation and sputtering from Cu nanowires under low-keV irradiation. Greaves *et al.* [18] present experiments and accompanying computer simulations for the sputter yield enhancement during the bombardment of Au nanorods under 80 keV Xe irradiation. Nietiadi *et al.* [19] present MD simulations and an analytical model for the sputtering of Si nanowires under low-keV ion impact.

While the effect of the surface tilt on the sputter yield has long been known [20,21], recently also the effect of the surface curvature on sputtering has been discussed, but only for central impacts [19]. This effect has now also been incorporated into the theory of pattern formation by irradiation [22].

Here we use MC simulation in the binary collision approximation to systematically study the deviations of sputtering between a planar surface and spheres of various radii. For relatively large sphere radii, the deviations from the well-understood sputtering of a planar surface can be easily interpreted and quantified. These deviations are due to oblique ion impact and target curvature. For smaller radii, the sputter yield passes through a maximum and then decreases again when $R \to 0$. For smaller spheres we use MD to corroborate our findings.

II. METHOD

MC simulation is an established method to study sputtering in the collision-cascade regime [23,24]. The presently employed code TRI3DST makes use of collisional algorithms, which are taken from the sputter version TRIM.SP [25] of the widely used TRIM code [26,27], with several modifications as described in a recent paper on three-dimensional (3D) dynamic simulations [28]. Basically, the propagation of incident projectiles and generated recoils in an amorphous medium (thus being appropriate for an a-Si target) is traced as a sequence of

*urbassek@rhrk.uni-kl.de

 ©2014 American Physical Society

binary collisions in a repulsive screened Coulomb potential with the Kr-C parametrization [29]. Electronic stopping is included as an equipartition of nonlocal (according to Lindhard and Scharff [30]) and local (according to Oen and Robinson [31]) energy losses. TRI3DST is applicable to homogeneous three-dimensional multicomponent bodies, the surface of which can be described by an analytical function. For the transmission of sputtered atoms through the surface, a local planar surface barrier is assumed with the local surface normal being deduced from the analytical contour function. Thereby, any dependence of the surface binding energy on the local curvature is not taken into account. The surface binding is set to $U = 4.7$ eV in accordance with the enthalpy of sublimation of Si.

Specifically, we model the sputtering of a planar a-Si target and of a-Si spheres of various radii R by 20 keV Ar ions. Data are based on 10^5 impacts for each combination of cluster radius and impact parameter (impact angle).

In addition, we perform MD simulations for small clusters, $R \leqslant 3.5$ nm, and only for central impact. In short, spherical clusters are cut out of an a-Si target that was prepared according to the recipe of Luedtke and Landman [32]. Silicon atoms interact via the Stillinger-Weber potential [33]. For small interaction distances the potential is fitted to the Ziegler-Biersack-Littmark (ZBL) potential [34]. Ar and Si atoms interact via the ZBL potential. In each case 1000 impacts have been simulated for a time of 3 ps. The impacts differed in that in each case a different impact point was chosen at random on the sphere, for normal impact angle. All atoms that are a distance of > 7.54 Å from the original sphere surface (that is twice the cutoff radius of the Stillinger-Weber potential) are considered as sputtered. Analogous MD simulations have also been performed for a flat target at normal incidence. Here the target consists of 35152 atoms, has a depth of 70 Å and a lateral extension of 100×100 Å^2.

III. RESULTS

In the following we first present and discuss the information obtained from the MC calculations; the comparison with MD data is given in Sec. III E.

The MC simulations give us basic information on the energy deposition profile in a planar target for normal incidence. In the usual ellipsoidal approximation [21] it is described by a Gaussian with center at the mean depth a below the surface and longitudinal and lateral RMS widths α and β, respectively, see Fig. 1. We obtain from the flat-target simulations $a = 208.9$ Å, and $\alpha = 123.0$ Å, $\beta = 79.7$ Å from the respective second central moments of the generated spatial distributions. This is in close agreement with the estimates obtained from the range distribution data provided by the SRIM software [27,35] and corrected by the factors given in Ref. [36]: $a = 213$ Å, $\alpha = 106$ Å, $\beta = 70$ Å. In the following we shall use the data obtained by our code.

A. Flat target: Infinitely large spheres

Figure 2 demonstrates that the position of impact on a sphere of radius R can be identified using the impact parameter b or alternatively the incidence angle ϑ (measured with respect to the local surface normal). In the following it will be useful to introduce the reduced impact parameter $x = b/R$. It is related to ϑ via

$$x = \sin\vartheta. \tag{1}$$

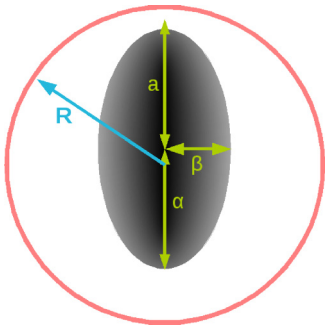

FIG. 1. (Color online) Sketch of the spherical cluster of radius R and the energy deposition profile, defining the parameters a, α, and β.

We shall denote the sputter yield of a sphere of radius R by Y_R; an infinitely large sphere has a sputter yield of Y_∞.

For large spheres, $R \gg a$, the sphere can be considered locally flat, such that only the angle of incidence influences the sputter yield. Figure 3(a) displays the sputter yield of a flat target as a function of incidence angle, and Fig. 3(b) converts these data by Eq. (1) to a function of the impact parameter of a sphere. While the sputter yield for normal incidence is $Y_\infty(x = 0) = 1.381$, sputtering is maximum at incidence angles of 80° where it reaches $Y_\infty(80°) = 11.26$. Such impacts correspond to glancing impact parameters of $x = 0.985$. The general shape of the angular dependence displayed in Fig. 3(a) is typical, while details such as the exact position of the maximum and the height of the maximum vary with ion-target combination and impact energy [24].

It is useful to introduce an average sputter yield of a sphere as

$$\langle Y_R\rangle = \frac{1}{\pi R^2}\int_0^R Y_R(b)2\pi b\,db = \int_0^1 2x\,dx\,Y_R(x). \tag{2}$$

This average has the meaning that a unidirectional flux Φ of projectile ions sputters a number of $\pi R^2\Phi\langle Y_R\rangle$ atoms from the sphere.

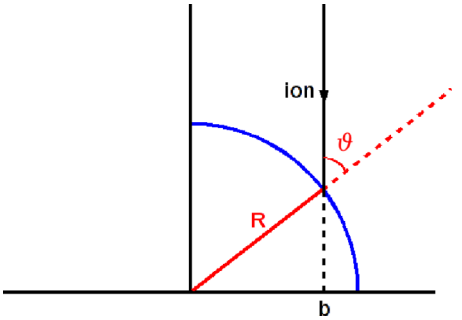

FIG. 2. (Color online) Impact of an ion on a sphere of radius R. The ion impinges at an impact parameter b and has a local incidence angle of ϑ.

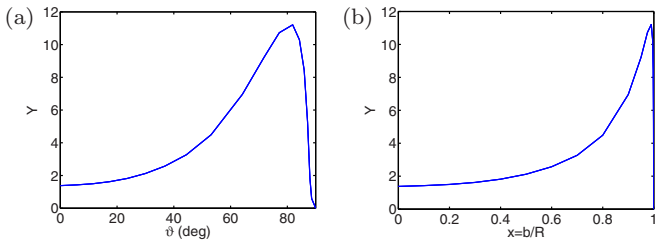

FIG. 3. (Color online) (a) Dependence of the sputter yield of a planar surface on the angle of incidence ϑ. (b) The same data interpreted as the sputter yield of a large sphere, radius $R \to \infty$, as a function of the reduced impact parameter $x = b/R$.

For the infinitely large sphere we obtain $\langle Y_\infty \rangle = 4.385$; this is a factor of 3.2 larger than the value at central impact. This is due to the large sputter yield increase at peripheral impact caused by the oblique incidence angle.

B. Effect of curvature

Figure 4(a) describes how the sputter yield of a sphere of radius R differs from an infinitely large sphere. To this end we plot the ratio $Y_R(x)/Y_\infty(x)$ as a function of the reduced impact parameter $x = b/R$. For large spheres, $R/a = 20$ and 10, $Y_R(x)$ grows above the values of Y_∞ homogeneously for all impact parameters; the changes increase with decreasing radius R.

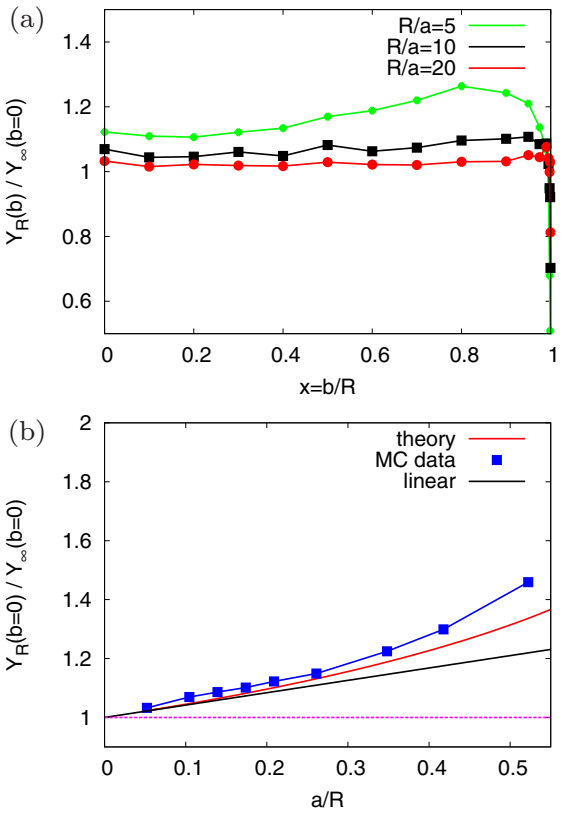

FIG. 4. (Color online) (a) Ratio of the sputter yield of a sphere of radius R, Y_R, to the sputter yield of an infinite sphere, Y_∞, as a function of the reduced impact parameter $x = b/R$. (b) Sputter yields for central impact, impact parameter $b = 0$, as a function of the inverse sphere radius, a/R. Data are normalized to the sputter yield of a flat target at normal incidence, $Y_\infty(b = 0)$. The theory curve, Eq. (A3), implements the result of a theoretical model presented in Appendix A and also the linearized result, Eq. (A7), is included. Data for large spheres, $R/a \geqslant 2$.

This overall increase is connected to the curvature of the sphere. The surface is curved in a convex way around the ion impact point; this leads to a larger energy deposition at the surface, increasing sputtering. The curvature dependence of the sputter yield has been analyzed recently for central impacts, $b = 0$ [19]. Sputtering has been found to be increased in comparison to a flat target. In first approximation, the enhancement depends only on one appropriately defined dimension-free curvature parameter κ, which depends on the geometry of the deposited energy distribution as

$$\kappa = \frac{a}{R}\left(\frac{\beta}{\alpha}\right)^2. \tag{3}$$

With the parameters given above, $\kappa = 0.42a/R$.

In Appendix A, we describe a simple model to calculate the sputtering yield of a sphere. It is based on linear collision cascade theory. Its basic assumption is that the energy deposition profile that is valid for a planar target also applies in the sphere. The sputter yield is then calculated as being proportional to the energy deposition integrated over the sphere surface.

Figure 4(b) compares the MC data for central impact with the prediction of the model, Eq. (A3), for sphere radii above $R/a \geqslant 2$. In this range the linear approximation, Eq. (A7), holds well. We see that up to $R/a \cong 4$, the linear increase describes the data reasonably well.

C. Effect of forward and lateral sputtering

Figure 5 demonstrates that for small spheres sputtering strongly deviates from Y_∞. The impact-parameter dependence of Fig. 5(a) demonstrates two effects. (i) For moderate sphere radii $R/a \cong 2$–5, sputtering disproportionately increases at large impact parameters, $x \cong 0.7$–0.8. (ii) For even smaller spheres, sputtering becomes maximum for central impacts.

The reason for the sputter maximum at peripheral impacts, $R/a = 2 - 5$, becomes evident when studying the emission-site distributions of Fig. 6. Here, two events are shown which lead to maximum sputter enhancement compared to Y_∞: $x = 0.8$ for $R/a = 4.77$ and $x = 0.7$ for $R/a = 1.91$. In both cases, sputter emission is not centered around the impact point, but considerable lateral and forward sputtering occurs. This is outside of the simple curvature effect described above: while the curvature is isotropic for a sphere, sputter emission is strongly anisotropic. The center of the deposited-energy distribution is below the impact point and comes into close vicinity of the lateral sphere surface.

Even for central impacts, the effect of curvature alone is not sufficient to describe sputtering. Figure 5(b) shows that sputtering follows well the simple model described in Appendix A up to around the sputter maximum. Sputtering reaches a maximum for $R \cong 0.5a$ for central impacts and then decreases again; in the model the maximum occurs slightly later, at $R \cong 0.7a$. Here the effect of forward sputtering is again responsible. Beyond the maximum—for small spheres—the

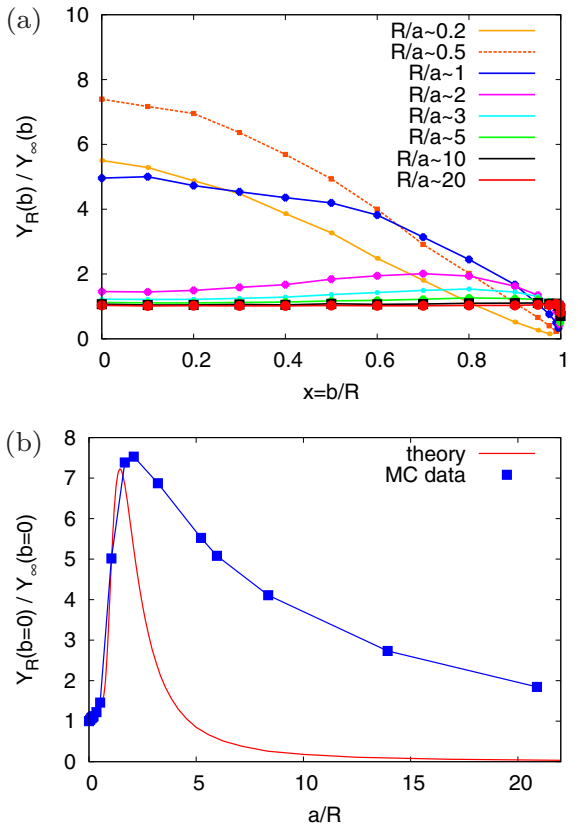

FIG. 5. (Color online) Same as Fig. 4, but for all spheres. The theory curve, Eq. (A3), in (b) implements the result of a theoretical model presented in Appendix A. The theory cannot describe sputtering of small spheres.

simple model completely fails and severely underestimates the sputtering. This failure is due to the basic assumption underlying the model: that the energy deposition profile is independent of the sphere radius.

Figure 7 shows how forward sputtering develops with decreasing sphere radius. For $R/a = 4.77$, no particles are emitted in forward direction, and Eq. (A3) gives a fair approximation of the sputter yield enhancement. Already for

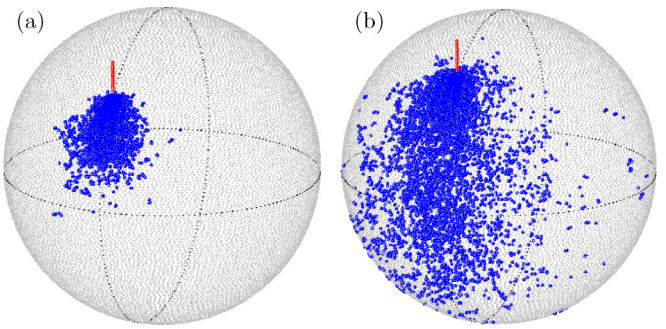

FIG. 6. (Color online) Emission-site distributions for oblique impact, (a) $R/a = 4.77$, $b/R = 0.8$ and (b) $R/a = 1.91$, $b/R = 0.7$. Direction of ion incidence and impact points are indicated by the red lines. The distributions have been obtained with 1000 incident projectiles.

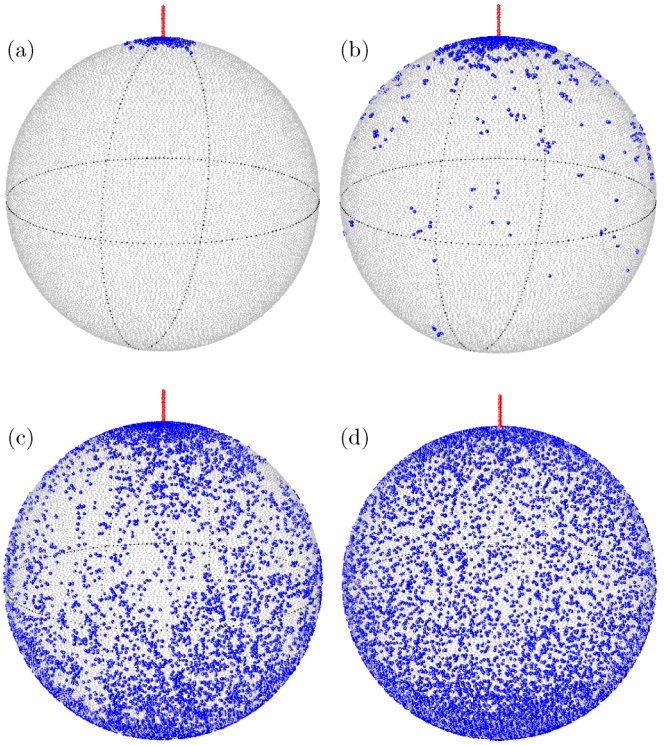

FIG. 7. (Color online) Emission-site distributions for central impact, $b = 0$: (a) $R/a = 4.77$, (b) $R/a = 1.91$, (c) $R/a = 0.95$, (d) $R/a = 0.19$. See Fig. 6 for further explanation.

$R/a = 1.91$ sputtering occurs from the forward hemisphere, and this effect becomes pronounced for $R/a = 0.95$; note that in that latter case forward sputtering is more important than sideways sputtering. This is due to the fact that the deposited-energy distribution is not spherical but elongated along the ion-impact direction, see Fig. 1. Only for the smallest sphere radius, $R/a = 0.19$, sputtering becomes isotropic, since here the sphere is filled more or less homogeneously with the deposited-energy profile. These results are in qualitative agreement with the theoretical model evaluated in Appendix A, Fig. 11.

D. Average sputter yield

Figure 8 displays the average sputter yield, Eq. (2). The main result here is that—in contrast to the yields for central impact—the average sputter yield enhancement is moderate, being smaller than a factor of 2.5. As evidenced by the impact-parameter resolved sputter data in Fig. 5(a), for spheres with radii $R \lesssim a$ sputtering is indeed maximum for central impact, but decreases monotonically for peripheral impacts. Since peripheral impacts are weighted strongly when averaging the sputter yield, Eq. (2), this explains why $\langle Y_R \rangle$ shows little enhancement while $Y(b = 0)$ increases strongly.

For large spheres, $R \gtrsim a$, $\langle Y_R \rangle$ increases roughly linearly with a/R as

$$\langle Y_R \rangle = \langle Y_\infty \rangle \left(1 + f \frac{a}{R}\right), \tag{4}$$

with a slope of $f = 1.25$. This is around a factor of 3 larger than the yield increase by the curvature effect; the extra increase is due to the forward sputtering described above.

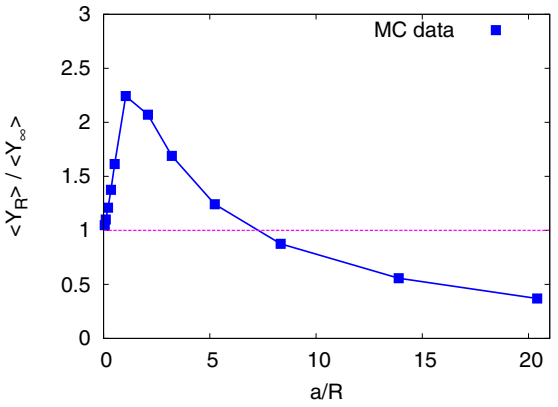

FIG. 8. (Color online) Average sputter yield, $\langle Y_R \rangle$, of a sphere of radius R, as a function of the inverse sphere radius, a/R.

The yield has a maximum at $R \cong a$; here the deposited energy fills out the sphere, maximizing sputtering. Note that for central impacts, $b = 0$, the yield becomes maximum only for smaller spheres $R = 0.5a$, see Fig. 5(b). This is due to the fact that forward sputtering is easier for peripheral impacts, which are counted with high weight in calculating the average sputter yield.

Finally, for $R < a$ the average sputter yield decreases again. In the literature two models for this decrease have been discussed.

(i) Järvi *et al.* [12] assume that the energy density in the sphere is the same as that close to the surface of a flat semi-infinite target. Since the sphere volume is $\propto R^3$, the energy deposited inside the sphere decreases $\propto (E R^3)$ with shrinking sphere radius R. This reasoning is analogous to the model outlined in Appendix A, Eq. (A9), and leads to

$$\langle Y_R \rangle \propto R^2. \tag{5}$$

(ii) In a later paper, [13], the authors assume that the energy deposited in the sphere varies linearly with R, since the nuclear stopping power can be assumed constant for small path lengths. This leads to

$$\langle Y_R \rangle = \text{const}, \quad (R \to 0). \tag{6}$$

Figure 5(b) demonstrates that for small spheres, model (i) as quantified by Eq. (A3) clearly fails. In addition, for the smallest cluster sizes, $R/a \leqslant 1$ the impact-parameter dependence of the sputter yield, Fig. 5(a) looks roughly like $\propto \sqrt{1 - x^2}$, and is thus proportional to the length of a straight projectile trajectory in the cluster. This speaks in favor of (ii) above and would lead to a constant average sputter yield for $R \to 0$. However, in this limit the number of atoms in the sphere also goes to 0, and thus the sputter yield becomes ill defined.

The MC data of the average sputter yield (see Fig. 8) show that indeed the sputter yield continuously decreases when the sphere radius is decreased below $R \lesssim a$. For spheres as small as $R \cong 0.2a$, the average sputter yield is still higher than for the infinite target. For even smaller spheres it steadily decreases.

E. MD results for small spheres: Importance of collision spikes

For the smallest spheres studied we might exceed the validity range of the MC model, and more realistic MD simulations should be performed. Collision spikes [37–39] may lead to abundant sputtering. In addition, at such highly curved surfaces the surface binding energy of atoms may be lowered; finally, the cluster may be totally fragmented if a high energy happens to be deposited due to a near-central collision of the projectile with a cluster atom. These effects are naturally included in MD.

We compare our MD data for spheres of radius $R =$ 1–3.5 nm with the MC data in Fig. 9; only central collisions are simulated. Note that the smallest sphere only contains 202 atoms. The MD data yield consistently larger yields than the MC data. Let us first discuss the sputter yields of a flat surface (at normal incidence). MD obtains 1.672 ± 0.067 when MC yields 1.381, a difference of 21 %. Here, it has to be noted that the Stillinger-Weber potential employed in MD produces a surface binding energy or 4.34 eV, being smaller than the value adopted in MC (4.7 eV). Further, the present MD simulations neglect energy dissipation due to interaction with the target electrons. Correspondingly, modified MC simulations have been performed (see Fig. 9) in which the surface binding energy was adjusted to the MD value, and electronic energy loss was suppressed. These data have been included in Fig. 9. For the flat target, the sputter yield increases to 1.904, even above the MD data. We note that we also performed an additional set of MC simulations in which the ZBL potential—as used in the MD simulations—was adopted rather than the Kr-C potential routinely used in our MC code. The deviations were below 5% for all sphere radii. In the MC simulations, systematic uncertainties arise from the choice of the interaction potential and the bulk binding energy (see Ref. [25]), and the questionable validity of the binary collision approximation [40] towards low kinetic energies of cascade atoms, which dominate sputtering. From this, an accuracy of better than about 20% can hardly be expected. In this light, the agreement of the flat target yields obtained by MD and MC must be considered as excellent.

For the spheres, however, larger systematic deviations are evident from Fig. 9. The data do not suggest a major influence of the surface binding energy, which might decrease with curvature, as this would increase the MC results in particular at small radii. Thus, we attribute the difference to the occurrence of collision spikes in the irradiated spheres; these are highly energized regions in the target where the basic assumptions of the MC simulation—viz. that atoms collide only with nonmoving atoms—are no longer satisfied. In regions of high local energy density (temperature) abundant sputtering can be induced. For small spheres, energy confinement arising from inner reflection of recoils, which hit the walls at glancing incidence, is expected to be more efficient than for the flat surface, as it occurs in all directions. This might assist the formation of spikes. Due to the high surface/volume ratio, the effect of spikes will be increased in small spheres. Indeed, from the MC simulations we calculate that the energy density deposited in the sphere assumes values of 0.1 eV/atom for the 4-nm spheres but increases to almost 0.2 eV/atom for the 1-nm sphere. These values emphasize that with decreasing sphere

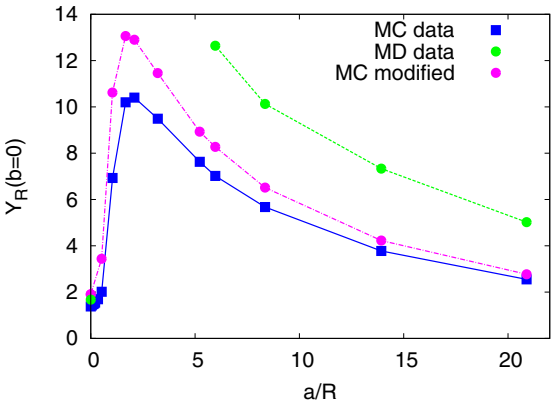

FIG. 9. (Color online) Absolute sputter yields for central impact, impact parameter $b = 0$, as a function of the inverse sphere radius, a/R. The MC data are supplemented by MD calculations. The MC modified data set has been obtained with an adjusted surface binding energy of 4.34 eV and under suppression of electronic interaction. See discussion in text.

size a stronger spike contribution to sputtering is expected. We give further evidence of the appearance of spike sputtering in Appendix B, where we compare the sputter yield distributions for the flat target and the spheres and emphasize the agreements and differences between the MC and MD data.

In order to demonstrate the action of spikes, Fig. 10 illustrates the sputter process in the MD simulation by giving a number of snapshots of the clusters at 3 ps after ion impact. The top row shows representative events in which the average number of atoms has been sputtered; the bottom row shows particularly abundant sputter events. We see that for the small spheres even for average energy deposition in the sphere, temperatures at and above the melting temperature of Si, 1687 K, are reached. For extreme energy depositions, and consequently extremely abundant sputtering, however, temperatures up to 5000 K are attained, which will at later times further fragment the clusters leading to later evaporation events. This series of snapshots explains the high sputter yields reached for small clusters. It demonstrates how the high-energy deposition leads to strong collision spikes that increase the sputter yields systematically beyond those of the MC calculations.

Strong yield enhancements in nanosized objects have been observed previously in simulations. Greaves *et al.* [18] describe a similar sputter yield enhancement during the bombardment of Au nanorods. Our series of snapshots demonstrates the high sputter yields reached for small clusters particularly in events with energy deposition largely above the average. Note, however, that the effect of spikes to the average sputter yield is moderate and amounts to a factor of less than 2.

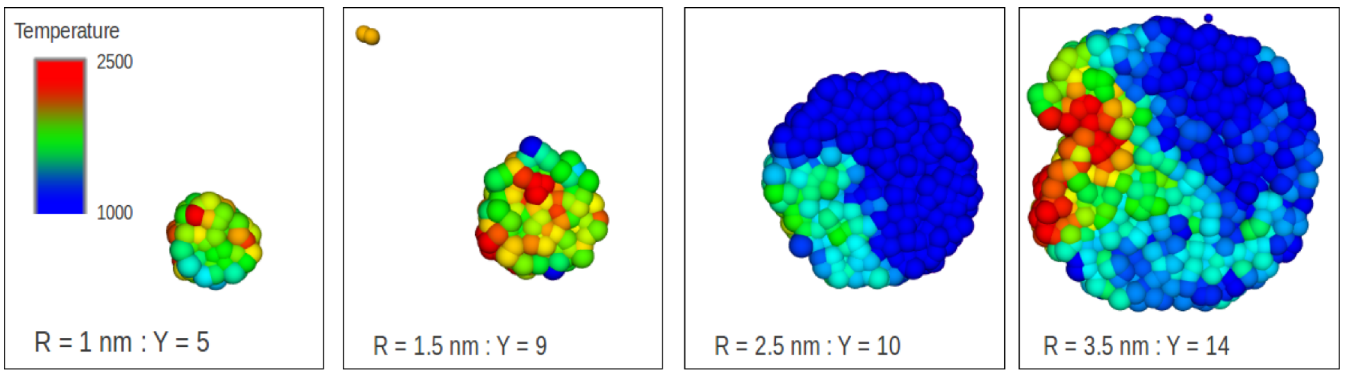

(a)

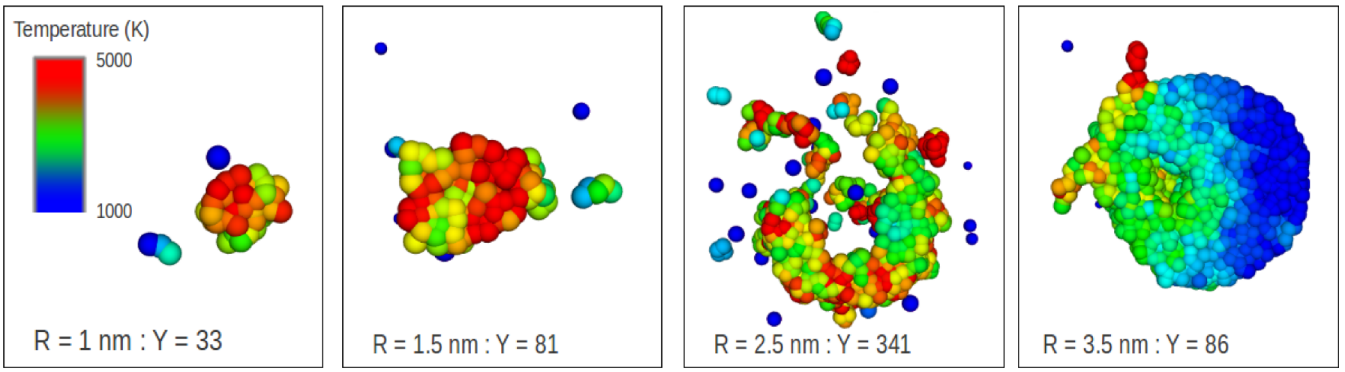

(b)

FIG. 10. (Color online) Cross-sectional view through the sputtered spheres at 3 ps after ion impact. Atoms are colored according to local temperature. (a) Representative events where impact leads to the average sputter yield. (b) Events with abundant sputtering. Note the change in color code between (a) and (b).

IV. CONCLUSIONS

We performed a dedicated MC study of sputtering of a-Si spheres of various radii R by 20 keV Ar impact. The radius R needs be set in proportion to the depth of energy deposition in the target, a. We expect that within the limits of collision-cascade theory our results can be qualitatively generalized to other irradiation conditions provided the ratio R/a is the same. Our study allows the following conclusions.

(i) For large radii $R \gg a$, the sputtering of a sphere can be quantitatively described by using data for the sputtering of a planar target, if the varying angle of incidence is taken into account. The average sputter yield of a sphere is always larger than that of a planar surface at normal incidence, since oblique incidence angles, which occur when a sphere is sputtered at peripheral impact parameters, lead to larger sputtering yields than normal impact.

(ii) For smaller radii, the curved surface increases the sputter yield, since the cluster surface comes closer to the deposited energy profile. For moderate curvatures, this effect is well modeled by a recent theory of curvature-dependent sputtering.

(iii) At still smaller radii, $R/a \lesssim 2$ lateral and forward sputtering increasingly contribute to the yield; this occurs at first at peripheral impacts, but at $R/a \cong 1$ extends also to central impacts.

(iv) At $R/a \cong 1$ the average sputter yield is maximum. Here the collision cascade fills the entire cluster and thus the energy deposition throughout the sphere surface is maximum.

(v) For even smaller clusters, $R/a < 1$ sputtering becomes isotropically distributed throughout the sphere surface. Yet the average sputter yield decreases again since not all the projectile energy is deposited in the sphere and furthermore the sputter surface decreases. However, even for the small spheres, $R = 0.2a$, the average sputter yield is still above that of an infinitely large sphere.

(vi) A simple model based on linear collision cascade theory and assuming that the energy deposition profile is independent of the sphere size predicts sputtering for large spheres well, but fails for small spheres where it strongly underestimates sputtering.

(vii) The average sputter yield of a sphere is less sensitive to the sphere radius than the sputter yield for central impacts. This is due to the compensation of two effects: For small spheres, the sputter yield increases at central impact but decreases for peripheral impacts.

(viii) Our MD simulations, performed for small spheres, corroborate the trend that the sputter yield saturates for small sphere radii. Compared to the MC data, the MD yields are systematically larger, indicating a contribution from collision spikes to sputtering.

ACKNOWLEDGMENTS

This work has been supported by the Deutsche Forschungsgemeinschaft via the Research Unit 845 *Self-organized nanostructures induced by low-energy ion beam erosion*.

APPENDIX A: THEORETICAL MODEL

In this Appendix we provide a theoretical description of sputtering from a sphere, based on linear-sputtering theory [21]. We focus on central impacts, $b = 0$, such that the problem is axially symmetric. Assume the origin of a cylindrical coordinate system to be situated at the ion impact point; z denotes the axial coordinate measuring the depth into the sphere, and r the radial coordinate. The surface of the sphere is then described by

$$z = h(r) = R \pm \sqrt{R^2 - r^2}, \tag{A1}$$

such that "–" denotes the upper and "+" the lower hemisphere. The energy deposited in low-energy recoil motion in the target at a point $\boldsymbol{r}$ is denoted as the deposited-energy profile $F_D(\boldsymbol{r})$. It is commonly approximated by a Gaussian function [21,36,41]

$$F_D(z,r) = \frac{E}{(2\pi)^{3/2}\alpha\beta^2} \mathrm{e}^{-(z-a)^2/(2\alpha^2)-r^2/(2\beta^2)}. \tag{A2}$$

The parameters a, α, and β were already introduced in Sec. III above, see also Fig. 1. Linear sputter theory assumes the sputter yield to depend on the deposited energy in the sphere as [41]

$$Y_R = \Lambda \int_0^R F_D[z = h(r), r] \sqrt{1 + h'^2(r)}\, 2\pi r\, dr, \tag{A3}$$

where Λ is a material parameter. Here $h'(r)$ denotes the slope of the surface and the term $\sqrt{1 + h'^2}$ represents the relative increase of the sphere surface with respect to the projected area $2\pi r dr$. For the sphere, the sputter yield can be decomposed into a contribution from the upper hemisphere [+ sign in $h(z)$, Eq. (A1)] denoting backward sputtering, and the analogous forward sputtering contribution. We found no way to solve the integral in Eq. (A3) analytically and therefore calculate it numerically. The sphere sputter yields are shown in Fig. 11 for the parameters pertinent to the present problem ($a = 208.9$ Å, $\alpha = 123.0$ Å, $\beta = 79.7$ Å), along with their decomposition into forward and backward sputtering. We see that for large spheres only back sputtering is relevant; forward sputtering sets in at $a/R \cong 0.63$, where $Y_R(b = 0)/Y_\infty(b = 0)$ reaches values >0.01. For smaller sphere radii, forward sputtering becomes more important than backward sputtering; this appears natural as the projectile

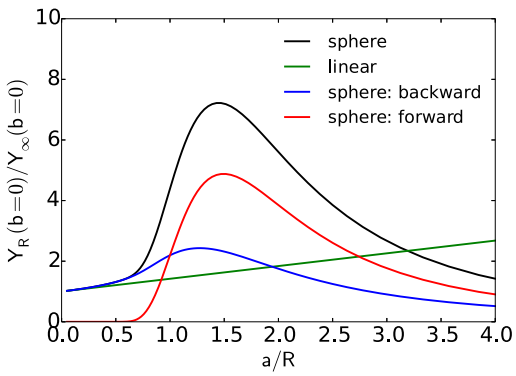

FIG. 11. (Color online) Result of a theoretical model, Eq. (A3), for the sputter yield for central impact, impact parameter $b = 0$, as a function of the inverse sphere radius, a/R. Data are normalized to the sputter yield of a flat target at normal incidence, $Y_\infty(b = 0)$. A linear approximation, Eq. (A7), valid for large spheres, $a/R \ll 1$, is added. In addition, the sphere yield is separated into its forward and backward sputtering contributions.

momentum is forward directed and can eject atoms more easily in the forward direction. The maximum of the sputter yield occurs at $a/R = 1.5$, close to the radius where forward sputtering is maximum.

The limit of large spheres, $a/R \to 0$, has been treated previously by approximating the sphere surface by a paraboloid [19]. In that paper, the term $\sqrt{1+h'^2}$ was omitted in calculating the sputter yield, Eq. (A3). When including it, no general analytical solution appears possible. However, the solution for large R/a—obtained as the first term of a series expansion in a/R—remains valid, as we shall now show. For large radii, only the upper hemisphere sputters, and Eq. (A1) can be approximated as a paraboloid

$$h(r) = \frac{r^2}{2R}. \tag{A4}$$

Equation (A3) then gives

$$Y_R = Y_\infty \frac{1}{\beta^2} \int_0^\infty \sqrt{1+\left(\frac{r}{R}\right)^2} \exp\left\{-\frac{r^2}{2\beta^2}\right\} \times \exp\left\{-\frac{1}{2\alpha^2}\left[\left(\frac{r^2}{2R}\right)^2 - \frac{ar^2}{R}\right]\right\} r\,dr, \tag{A5}$$

where we have increased the upper integration limit to ∞, which is fine for $R \gg \beta$. Expanding the integrand in a/R and keeping only linear terms we arrive at

$$Y_R = Y_\infty \frac{1}{\beta^2} \int_0^\infty e^{-r^2/(2\beta^2)} \left(1 + \frac{a}{R}\frac{r^2}{2\alpha^2}\right) r\,dr. \tag{A6}$$

In summary,

$$Y_R(b=0) = (1+\kappa)\cdot Y_\infty, \quad R \to \infty, \tag{A7}$$

where κ is a dimensionless curvature parameter,

$$\kappa = \frac{a}{R}\left(\frac{\beta}{\alpha}\right)^2. \tag{A8}$$

We include this linear approximation in Fig. 11. It describes the sphere well up to $a/R = 0.35$; then the sphere sputter yield increases more strongly than predicted by the linear result. In the limit of small spheres, Eq. (A3) gives

$$Y \cong Y_\infty(b=0)\cdot 2\left(\frac{R}{\beta}\right)^2, \quad R \to 0. \tag{A9}$$

The dependence on α is absorbed in $Y_\infty(b=0)$. However, the use of the model in this limit is not realistic. Note that the essential assumption underlying this model consists in the use of Eq. (A3) also for nanometric sputter targets, when the target size becomes of the order or even smaller than the radius of the energy deposition zone, a. The model assumes here that the energy deposition profile remains unchanged from that of an extended solid, as given by Eq. (A2). As we show in the main text, our MC and MD simulations give good agreement with the theory results for large spheres, but show strong deviations for small spheres; these show that the model presented here loses its validity in the latter case.

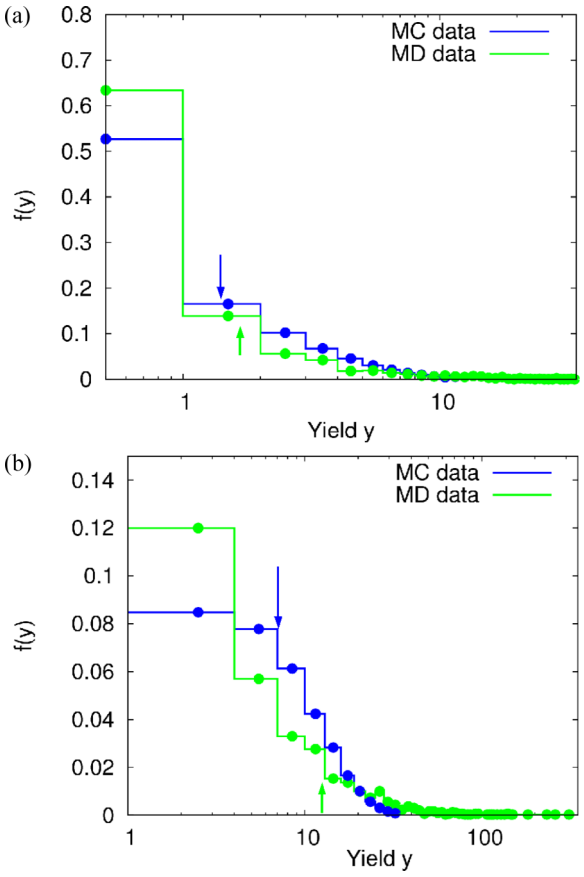

FIG. 12. (Color online) Comparison of the sputter statistics of MC and MD data obtained for the (a) flat target and (b) for the sphere with 3.5 nm radius. The average values are marked by arrows.

APPENDIX B: SPUTTER STATISTICS

The sputter yield is a stochastic quantity in the sense that it may assume a different value for each individual impact event. Let us denote by y the individual sputter yield and its average by $\langle y\rangle = Y$ as in the main part of the text. The distribution function $f(y)$ gives the probability with which a particular sputter yield y is observed in an individual event. This function is displayed in Fig. 12 for the MC and the MD data for two targets: the flat target and the sphere with 3.5 nm radius. The relevance of sputter statistics has been discussed previously in the literature, preferably for MC simulations [42–44].

For the flat target, Fig. 12(a), MC and MD are in fair agreement with each other. Most often, no particle is emitted, since the projectile deposits its energy deep in the target. If particles are emitted, the probabilities of emitting exactly y particles decrease quickly with increasing y. Note that the MD data show a slightly higher peak at $y = 0$ and decay faster with increasing y; this may appear astonishing since MD shows a slightly larger average yield (1.672 in MD, 1.381 in MC). But the long tail observed for the MD sputter distribution—the largest sputter yield observed was 34—increases the average yield. Such large-emission events are typical of spike sputtering. Overall however, we conclude that the fact that the two statistical distributions are quite

similar is an indication that also the physics of individual events is treated similarly in MC and MD.

Differences between the MC and MD distributions become stronger in the case of sputtering of small spheres, Fig. 12(b). In the case considered here, the average sputter yield was 7.017 for MC and 12.77 for MD. Let us first discuss the MC statistics. Here the distribution has considerably broadened with respect to the flat target. Such a behavior is to be expected since the average sputter yield increases, and the width of the sputter distribution is (roughly) of the same size as the average [42–44]. The physics reason both for the increased average yield and the increased width is that the sphere radius is already quite small in comparison to the deposited energy profile ($a \cong 5.969R$), such that ions as a rule penetrate the sphere leading to abundant emission on all locations of the sphere surface.

The MD distribution shows less broadening for the small yields; the probability that less than $y \lesssim 15$ particles are sputtered is smaller than in MC (with the exception of the probability that no atom is sputtered, $y = 0$). However, this relative lack of moderate sputter events is more than compensated by an increase of abundant sputter events; the largest sputter yield observed was 311. As shown in Fig. 10, these abundant sputter events are due to spike sputtering.

In summary, this comparison of sputter distributions corroborates the view that spike sputter events, with their abundant sputter yields, are responsible for the yield enhancement observed for small spheres in MD.

[1] T. A. Cassidy and R. E. Johnson, Icarus **176**, 499 (2005).
[2] E. M. Bringa, S. O. Kucheyev, M. J. Loeffler, R. A. Baragiola, A. G. G. M. Tielens, Z. R. Dai, G. Graham, S. Bajt, J. P. Bradley, C. A. Dukes *et al.*, Astrophys. J. **662**, 372 (2007).
[3] A. Bouchoule, Phys. World **6**, 47 (1993), No. 8.
[4] U. Kirchner, R. Vogt, C. Natzeck, and J. Goschnick, J. Aerosol Sci. **34**, 1323 (2003).
[5] T. T. Järvi, D. Pohl, K. Albe, B. Rellinghaus, L. Schultz, J. Fassbender, A. Kuronen, and K. Nordlund, Europhys. Lett. **85**, 26001 (2009).
[6] A. Klimmer, P. Ziemann, J. Biskupek, U. Kaiser, and M. Flesch, Phys. Rev. B **79**, 155427 (2009).
[7] R. E. Johnson, Space Sci. Rev. **69**, 215 (1994).
[8] R. Kissel and H. M. Urbassek, Nucl. Instrum. Meth. B **180**, 293 (2001).
[9] R. Kissel and H. M. Urbassek, Int. J. Mass Spectrom. **208**, 29 (2001).
[10] S. Zimmermann and H. M. Urbassek, Int. J. Mass Spectrom. **272**, 91 (2008).
[11] J. C. Jimenez-Sanz, A. M. C. Perez-Martin, and J. J. Jimenez-Rodriguez, Nucl. Instrum. Meth. B **316**, 210 (2013).
[12] T. T. Järvi, J. A. Pakarinen, A. Kuronen, and K. Nordlund, Europhys. Lett. **82**, 26002 (2008).
[13] T. T. Järvi and K. Nordlund, Nucl. Instrum. Meth. B **272**, 66 (2012).
[14] S. Jurac, R. E. Johnson, and B. Donn, Astrophys. J. **503**, 247 (1998).
[15] W. L. Chan and E. Chason, J. Appl. Phys. **101**, 121301 (2007).
[16] See the special section on *Surface nanopatterns induced by ion-beam sputtering* in J. Phys.; Condens. Matter. **21**, 220301 (2009).
[17] Z. Xue-Qing, X. Jian-Ming, and W. Yu-Gang, Chinese Phys. B **19**, 036102 (2010).
[18] G. Greaves, J. A. Hinks, P. Busby, N. J. Mellors, A. Ilinov, A. Kuronen, K. Nordlund, and S. E. Donnelly, Phys. Rev. Lett. **111**, 065504 (2013).
[19] M. L. Nietiadi and H. M. Urbassek, Appl. Phys. Lett. **103**, 113108 (2013).
[20] P. Sigmund, Phys. Rev. **184**, 383 (1969).
[21] P. Sigmund, in *Sputtering by particle bombardment I*, edited by R. Behrisch (Springer, Berlin, 1981), p. 9.
[22] M. P. Harrison and R. M. Bradley, Phys. Rev. B **89**, 245401 (2014).
[23] W. Eckstein and H. M. Urbassek, in *Sputtering by Particle Bombardment*, edited by R. Behrisch and W. Eckstein (Springer, Berlin, 2007), Vol. 110 of Topics Appl. Physics, p. 21.
[24] W. Eckstein, in *Sputtering by Particle Bombardment*, edited by R. Behrisch and W. Eckstein (Springer, Berlin, 2007), Vol. 110 of Topics Appl. Physics, p. 33.
[25] J. P. Biersack and W. Eckstein, Appl. Phys. A **34**, 73 (1984).
[26] J. P. Biersack and L. G. Haggmark, Nucl. Instr. Meth. **174**, 257 (1980).
[27] J. F. Ziegler, SRIM: http://www.srim.org/ (2000).
[28] W. Möller, Nucl. Instrum. Meth. B **322**, 23 (2014).
[29] W. D. Wilson, L. G. Haggmark, and J. P. Biersack, Phys. Rev. B **15**, 2458 (1977).
[30] J. Lindhard and M. Scharff, Phys. Rev. **124**, 128 (1961).
[31] O. S. Oen and M. T. Robinson, Nucl. Instr. Meth. **132**, 647 (1976).
[32] W. D. Luedtke and U. Landman, Phys. Rev. B **40**, 1164 (1989).
[33] F. H. Stillinger and T. A. Weber, Phys. Rev. B **31**, 5262 (1985).
[34] J. F. Ziegler, J. P. Biersack, and U. Littmark, *The Stopping and Range of Ions in Solids* (Pergamon, New York, 1985).
[35] J. F. Ziegler, Nucl. Instrum. Meth. B **219-220**, 1027 (2004).
[36] K. B. Winterbon, P. Sigmund, and J. B. Sanders, Mat. Fys. Medd. K. Dan. Vidensk. Selsk. **37** (1970), No. 14.
[37] P. Sigmund, Appl. Phys. Lett. **25**, 169 (1974); **27**, 52 (1975).
[38] H. H. Andersen, Mat. Fys. Medd. K. Dan. Vidensk. Selsk. **43**, 127 (1993).
[39] H. M. Urbassek, in *Ion Beam Science: Solved and Unsolved Problems*, edited by P. Sigmund (Royal Danish Academy of Sciences, Copenhagen, 2006), Vol. 52 of Mat. Fys. Medd. Dan. Vid. Selsk., p. 433.
[40] W. Eckstein, *Computer simulation of ion-solid interactions* (Springer, Berlin, 1991).
[41] P. Sigmund, J. Mater. Sci. **8**, 1545 (1973).
[42] W. Eckstein, Nucl. Instrum. Meth. B **33**, 489 (1988).
[43] U. Conrad and H. M. Urbassek, Nucl. Instrum. Meth. B **48**, 399 (1990).
[44] M. T. Robinson, Nucl. Instrum. Meth. B **90**, 509 (1994).